





Multiphysics Modeling for Transient Analysis of Gas-Insulated Lines

Dimitrios I. Doukas , *Member, IEEE*, Theofilos A. Papadopoulos , *Senior Member, IEEE*,
Andreas I. Chrysochos, *Member, IEEE*, Dimitris P. Labridis , *Senior Member, IEEE*,
and Grigoris K. Papagiannis , *Senior Member, IEEE*

Abstract—In this paper, two discretization techniques are combined to present a coupled electro-thermal model for the transient analysis of gas-insulated transmission lines (GILs). The analysis of the thermal problem is based on the volume-element-method, representing heat transfer equations on a 2-D axisymmetric GIL model and determining temperature distribution over space and time. For the electrical formulation, the finite-difference time-domain method is adopted considering constant parameters calculated at the frequency of interest. The coupled electro-thermal problem in the case of transient conditions is solved by means of a bidirectional procedure. A set of test cases is imposed on the electric part, and transient analysis is conducted while considering the line coupled electro-thermal performance.

Index Terms—Coupled electro-thermal modeling, finite-difference time-domain (FDTD), gas-insulated transmission line (GIL), short-circuits, transients, volume-element-method (VEM).

I. INTRODUCTION

GAS-INSULATED lines (GILs) were proposed as an alternative transmission system due to their distinct characteristics in densely populated and environmentally protected areas or in conjunction with other infrastructure projects, e.g., hydropower dams, gas or oil power plants, etc. [1]. The main advantages of GILs are the low transmission losses, similar operation and power rating characteristics to overhead lines, the increased safety and operation aspects, such as limited need for reactive compensation, non-aging characteristics of gases and reduced electromagnetic fields [1].

Manuscript received November 3, 2017; revised January 30, 2018; accepted March 23, 2018. Date of publication March 27, 2018; date of current version November 20, 2018. The work of A. I. Chrysochos was conducted in the framework of the act “Support of Post-Doc Researchers” under the Operational Program “Human Resources Development, Education and Lifelong Learning 2014–2020,” which is implemented by the State Scholarships Foundation and co-financed by the European Social Fund and the Hellenic Republic. Paper no. TPWRD-01350-2017. (*Corresponding author: Dimitrios Doukas.*)

D. I. Doukas, D. P. Labridis, and G. K. Papagiannis are with the School of Electrical and Computer Engineering, Aristotle University of Thessaloniki, 54124 Thessaloniki, Greece (e-mail: doux@auth.gr; labridis@auth.gr; grigoris@eng.auth.gr).

T. A. Papadopoulos is with the Power Systems Laboratory, Department of Electrical and Computer Engineering, Democritus University of Thrace, 67100 Xanthi, Greece (e-mail: thpad@ee.duth.gr).

A. I. Chrysochos is with the Cable Hellenic Cables S.A., Viohalco Group, Sousaki Korinthias, 20100 Korinthos, Greece (e-mail: achrysochos@fulgor.vionet.gr).

Color versions of one or more of the figures in this paper are available online at <http://ieeexplore.ieee.org>.

Digital Object Identifier 10.1109/TPWRD.2018.2820022

The first GIL application is the 400-kV, 700-m GIL at Schluchsee hydropower plant in Germany that went in service in 1975, while one of the longest GILs in the world is the 3.3 km Shinmeika-Tokai line in Japan, operating at 275 kV [2], [3]. Since 1975, a number of GIL installations have been constructed at different voltage levels, types of applications, climatic conditions and structures, e.g., in substations, tunnels, railway or highway galleries [1].

Despite the proven technical feasibility of GILs, several studies have addressed a series of issues considering their installation and operation. Therefore, heat transfer characteristics of GILs under varying temperature conditions were studied in [4]–[6], while [7]–[12] focus on technical aspects, such as insulation coordination, maximum magnetic - electric field calculations and transmission line modeling. More advanced GIL electromagnetic and thermal models for the analysis of the coupled electro-thermal problem were introduced in [7], [10] and [13], using either detailed formulations or finite-element-method (FEM) [14]–[16].

On the other hand, transient simulation techniques and computational tools are becoming increasingly relevant to the design and analysis of GIL systems. Reliable simulation tools are useful to provide a framework of secure operation and circumscribe limitations, difficult to identify even through experimental setups. Most simulation models reported in literature focus on the electromagnetic analysis of GILs to evaluate their performance under steady-state conditions [4]–[9], [11], [13]. Additionally, thermal analysis is vital to keep operating conditions within certain limits and prevent equipment damage.

This study has as scope to present a new fully coupled electro-thermal solution for the transient analysis of GILs. The proposed model is generic and can serve as an efficient simulation and design mechanism for the prediction of the thermal behavior of any GIL under transient conditions and to identify an overall framework of secure operation. For this purpose, two widely accepted and well validated discretization techniques are combined, i.e., the volume-element-method (VEM) [17] for the thermal analysis and the finite-difference time-domain (FDTD) [18], [19] for the electrical analysis. The heat transfer equations are analyzed in 2D, using the flexible parabolic-elliptic partial differential equations (PDEPE) solver [20] of MATLAB [21], to calculate the temperature distribution of all GIL layers in space and time. The transient performance

of a GIL configuration is investigated considering both slow and fast transient response calculations [3].

In Sections II and III, the thermal and electric problem formulation are presented, respectively. In Section IV, the procedure for the electro-thermal modeling is given, while Section V introduces details related to the case study and GIL modeling. Sections VI and VII are devoted to results and the analysis of the discretization efficiency. Finally, in Section VIII the main conclusions of this paper are summarized.

II. THERMAL ANALYSIS

The problem in this case is initial-boundary value for varying space z and time t that can be expressed by partial differential equations (PDEs) that represent the laws of thermodynamics and heat transfer. In this context, the generic expression of (1) is employed and the PDEPE solver of MATLAB is utilized.

$$c \left(z, t, T, \frac{\partial T}{\partial z} \right) \frac{\partial T}{\partial t} = z^{-m} \frac{\partial}{\partial z} \left[z^m f \left(z, t, T, \frac{\partial T}{\partial z} \right) \right] + s \left(z, t, T, \frac{\partial T}{\partial z} \right). \quad (1)$$

Start and stop time-instances of the simulation are represented by t_0 and t_f , respectively, whereas a and b correspond to the GIL sending and receiving ends. Depending on the symmetry utilized, m can be 0 for slab, 1 for cylindrical and 2 for spherical symmetry.

Flux $f(z, t, T, \frac{\partial T}{\partial z})$ and source $s(z, t, T, \frac{\partial T}{\partial z})$ terms illustrate heat transfer on z and r directions, respectively, and their definition is crucial to the solution of the PDEs system. Moreover, multiplication with $c(z, t, T, \frac{\partial T}{\partial z})$ on the left side of (1) enables the coupling of the partial derivatives over space z , $\frac{\partial T}{\partial z}$, with respect to time. Elements of c are positive in case of parabolic equations and zero for elliptic ones [20]. T corresponds to the temperature distribution over space and time, and combined with the $\frac{\partial T}{\partial z}$ are the outputs of this formulation. On the other hand, inputs can be considered the scalars z and t .

Application of VEM in case of GIL layers enables the simultaneous discretization over time t and space z , by dividing all layers of the GIL configuration in VEs. Then, a group of PDEs that represents heat transfer across consecutive VEs in both radial and axial directions is solved to illustrate temperature distribution, for all layers, over GIL length and for varying time t .

Expressions that describe heat transfer by any means, i.e., conduction, convection and radiation are presented, based on the analysis of [17], [22] in order to make the proposed model as generic as possible. However, in this work heat transfer by convection does not occur, since no flowing liquids or gases are involved. Equations (2)–(8) describe the discretization approach and the heat transfer model used in this work.

A. Conduction

Regardless of the direction, between consecutive solid VEs only transfer by conduction takes place.

On z direction, for the l th GIL layer that is made of a material with thermal conductivity k_l and for a cross-section $A_{r,l}$, heat conduction across three VEs in a row is given by

$$\begin{cases} \dot{Q}_{l,d,in}^i = -\frac{k_l A_{r,l} (T_{l-1}^i - T_l^{i-1})}{\Delta_z^{i-1}} \\ \dot{Q}_{l,d,out}^i = -\frac{k_l A_{r,l} (T_l^{i+1} - T_l^i)}{\Delta_z^{i+1}} \end{cases} \quad (2)$$

Likewise, on r direction, the corresponding expressions for heat transfer by conduction between different l_1 and l_2 GIL layers and for neighboring VEs of the i th cross-section are

$$\dot{Q}_{l_1 l_2, d}^i = U_{l_1 l_2}^i (T_{l_2}^i - T_{l_1}^i) \quad (3)$$

where $U_{l_1 l_2}^i$ is

$$U_{l_1 l_2}^i = \left(\frac{\ln \frac{2R_{l_1}}{R_{l_1-1} + R_{l_1}}}{2\pi k_{l_1} \Delta_z^i} + \frac{\ln \frac{R_{l_1} + R_{l_2}}{2R_{l_1}}}{2\pi k_{l_2} \Delta_z^i} \right)^{-1}. \quad (4)$$

R_{l_1} , R_{l_2} and R_{l_1-1} refer to the radii of layers l_1 , l_2 and of the layer before l_1 , respectively. Equation (3) is used to calculate heat exchange from the environment, \dot{Q}_e , as well.

B. Convection

In case neighboring VEs are made of solid and liquid materials, heat transfer by convection can occur on both directions. Given that \dot{m}_l and c_{p_l} correspond to mass flow and specific heat, respectively, heat convection is calculated based on

$$\begin{cases} \dot{Q}_{l,v,in}^i = -\dot{m}_l c_{p_l} (T_l^i - T_l^{i-1}) \\ \dot{Q}_{l,v,out}^i = -\dot{m}_l c_{p_l} (T_l^{i+1} - T_l^i) \end{cases} \quad (5)$$

$$\dot{Q}_{l_1 l_2, v}^i = h_{l_1} A_{l_1, l_2}^i (T_{l_2}^i - T_{l_1}^i). \quad (6)$$

Considering Nusselt number Nu and hydraulic diameter D_h , h_{l_1} is given by

$$h_{l_1} = \frac{k_{l_1} Nu}{D_h}. \quad (7)$$

C. Radiation

Between the GIL conductor and the outer enclosure, SF_6 is imposed, therefore heat transfer by radiation also takes place. Taking into account that A_l^i refer to the cylindrical surfaces, heat radiation for adjacent VEs of the i th line cross-section between different l_1 and l_2 GIL layers, that surround SF_6 layer, on r direction is given by

$$\begin{cases} \dot{Q}_{r,in}^i = -\frac{\varepsilon_{l_1}}{1-\varepsilon_{l_1}} A_{l_1}^i [B_1 - \sigma (T_{l_1}^i)^4] \\ \dot{Q}_{r,out}^i = -\frac{\varepsilon_{l_2}}{1-\varepsilon_{l_2}} A_{l_2}^i [\sigma (T_{l_2}^i)^4 - B_2] \end{cases} \quad (8)$$

B_1 and B_2 are described in [17], whereas σ and ε are the Stefan-Boltzman constant and the material emissivity.

As mentioned, this is an initial-boundary conditions problem to solve, which is given by (9) and (10), respectively.

$$T(z, t_0) = T_0(z). \quad (9)$$

$$p(z, t, T) + q(z, t) f \left(z, t, T, \frac{\partial T}{\partial z} \right) = 0. \quad (10)$$

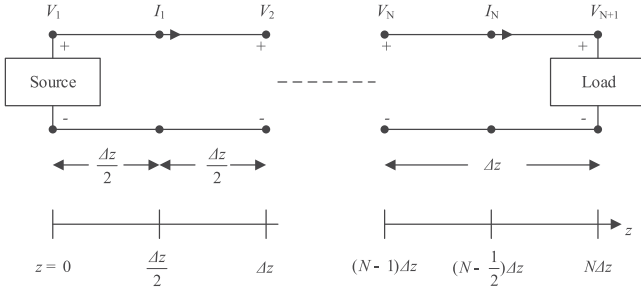


Fig. 1. GIL space discretization.

Temperature at $t = t_0$ and all z , i.e., along the GIL layers, is introduced as the initial condition in this study. Two boundary conditions are considered, which depend only on the flux term f and refer to all t and for each GIL configuration terminations, therefore either for $z = a$ or for $z = b$.

Equation (10) includes the vector functions p and q , which are time- and space-dependent, whereas p can also be solution-dependent. Finally, the elements of q can be either equal to zero or never zero.

III. ELECTRICAL FORMULATION

To calculate the transient voltage and current responses along the GIL, constant parameter (CP) FDTD modeling. CP FDTD modeling is selected to minimize simulation time, thus the 6×6 per-unit length (pul) resistance \mathbf{R}' , inductance \mathbf{L}' and capacitance \mathbf{C}' matrices of the GIL [23] are calculated at the frequency of interest, according to the examined test case [24]. The GIL is discretized into N sections of length Δz as shown in Fig. 1 [18]. Accordingly, the total simulation time is divided into M segments and the time step is Δt .

Based on FDTD, telegrapher's equations are solved in discrete form for all intermediate points of the line. Voltages and currents are calculated at each time step n by means of past solutions as shown in (11) and (12), respectively. Initially, zero values for both voltages and currents is assumed [25].

$$\mathbf{V}_k^{n+1} = \mathbf{V}_k^n - \left(\frac{\Delta z}{\Delta t} \mathbf{C}' \right)^{-1} \left(\mathbf{I}_k^{n+1/2} - \mathbf{I}_{k-1}^{n+1/2} \right) \quad (11)$$

for $k = 2, 3, \dots, N$.

$$\begin{aligned} \mathbf{I}_k^{n+3/2} = & \left(\frac{\Delta z}{\Delta t} \mathbf{L}' + \frac{\Delta z}{2} \mathbf{R}' \right)^{-1} \left(\frac{\Delta z}{\Delta t} \mathbf{L}' - \frac{\Delta z}{2} \mathbf{R}' \right) \mathbf{I}_k^{n+1/2} \\ & - \left(\frac{\Delta z}{\Delta t} \mathbf{L}' + \frac{\Delta z}{2} \mathbf{R}' \right)^{-1} \left(\mathbf{V}_{k+1}^{n+1} - \mathbf{V}_k^{n+1} \right) \end{aligned} \quad (12)$$

for $k = 2, 3, \dots, N$.

Finally, in order to include voltages V_1 and V_{NDZ+1} at the GIL ends, boundary conditions are applied, resulting into (13)

and (14), respectively.

$$\mathbf{V}_1^{n+1} = \left(\frac{\Delta z}{\Delta t} \mathbf{R}_S \mathbf{C}' + \mathbf{1}_n \right)^{-1} \left[\left(\frac{\Delta z}{\Delta t} \mathbf{R}_S \mathbf{C}' - \mathbf{1}_n \right) \mathbf{V}_1^n - 2\mathbf{R}_S \mathbf{I}_1^{n+1/2} + \left(\mathbf{V}_S^{n+1} + \mathbf{V}_S^n \right) \right] \quad (13)$$

$$\mathbf{V}_{N+1}^{n+1} = \left(\frac{\Delta z}{\Delta t} \mathbf{R}_L \mathbf{C}' + \mathbf{1}_n \right)^{-1} \left[\left(\frac{\Delta z}{\Delta t} \mathbf{R}_L \mathbf{C}' - \mathbf{1}_n \right) \mathbf{V}_{N+1}^n + 2\mathbf{R}_L \mathbf{I}_N^{n+1/2} + \left(\mathbf{V}_L^{n+1} + \mathbf{V}_L^n \right) \right] \quad (14)$$

where $\mathbf{1}_n$ corresponds to an identity matrix.

Simulations must be performed taking into account the “magic time step”, defined in (15), to satisfy the Courant Friedrichs Lewy (CFL) [26] condition and ensure stability.

$$\Delta t \leq \frac{\Delta z}{v} \quad (15)$$

In (15) is shown that Δt must be lower than the propagation time along each segment of the discretized GIL. Considering electromagnetic transients in aerial configurations, Δt can be selected assuming v equal to the speed of light c [19].

IV. COUPLED ELECTRO-THERMAL MODELING

To solve the coupled electro-thermal problem the bi-directional modeling procedure of Fig. 2 is proposed. Regarding the electrical problem, each GIL segment is represented by an electrical equivalent circuit, while the corresponding VE is formulated for the thermal problem.

Joule losses at the GIL metallic parts are represented by means of the heat generation $\dot{Q}_{g,1}$ defined in (16) for each GIL segment.

$$\dot{Q}_{g,1} = I_k^2 R'_k \quad (16)$$

where R'_k is the corresponding metallic part element resistance. Additionally, the variation of electrical resistivity against temperature T can be expressed by (17), assuming small temperature changes [27].

$$\rho(T) = \rho_0 [1 + \alpha(T - T_0)] \quad (17)$$

where α is the temperature coefficient of resistivity, i.e., $0.0039 \text{ } ^\circ\text{C}^{-1}$ for Al, T_0 is the reference temperature and ρ_0 is the resistivity at T_0 .

The coupling between the electrical and thermal problems is represented by the above set of equations, where the influence of current is translated into a heat event and consequently the variation of T affects the resistance of the metallic parts.

V. CASE STUDY & GIL MODELING

The examined case is based on [3], for long-distance GILs. The configuration is illustrated in Fig. 3. Mechanical support by means of supporting insulators that is typically used in GILs is not considered. All relative permeabilities equal 1.0, while the conductor and enclosure relative permittivity is 1.057 and 1.0, respectively.

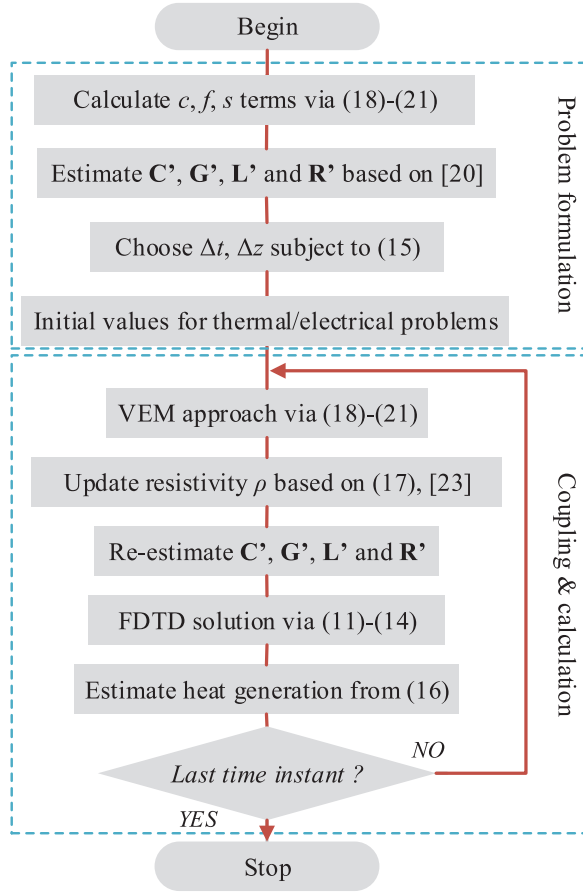


Fig. 2. Flowchart representation of the coupling process.

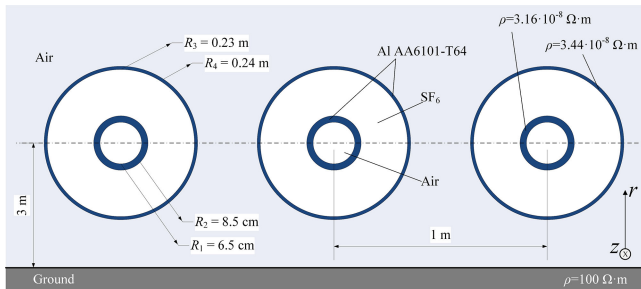


Fig. 3. GIL configuration cross-section.

The mathematical formulation can be easily extended and applied to any cross-section regardless its complexity. Such formulation is typically used in complex configurations where either gases [17] or liquids, as for example in case of liquid nitrogen-cooled superconducting cables are used [22]. Aluminum Al AA 6101-T64 is considered as the conducting material for both the GIL conductor and enclosure, while sulfur hexafluoride SF₆ is used for insulation. Even temperature distribution was considered, whereas the flow and expansion of SF₆ were not taken into account. For the inner pipe air is considered. In Table I, the material properties and initial conditions T_{init} are given in detail. The initial temperature of the surrounding environment

TABLE I
MATERIAL PROPERTIES AND INITIAL CONDITIONS

Material	k (W/m°C)	ρ (kg/m³)	c_v (J/kg°C)	T_{init} (°C)
Aluminum	226	2700	895	27
SF ₆	0.0136	6.2	56.928	27
Air	0.0257	1.225	718	27

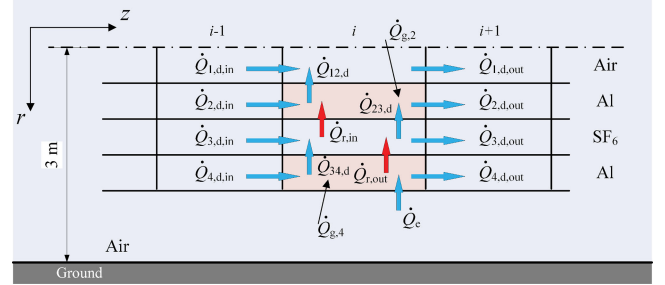


Fig. 4. Heat transfer approach and VE discretization.

equals 27 °C. Temperature conditions are within limits provided by IEEE in [28], [29].

In Fig. 4 arrows represent heat transfer between nearby VEs in both directions. For brevity, discretization for only one of the GIL phases is presented in Fig. 4, whereas the same analysis is applied on the other two phases as well.

The PDEs expressing the 1st law of thermodynamics are formulated for the i th VE of any layer, according to the examined GIL configuration and the heat transfer representation of Fig. 4. Since each GIL unit consists of 4 layers, 4 PDEs are considered. All PDEs are formulated by means of (1), considering terms c , f and s [30]. The flux term f correspond to heat transfer on the z axis, i.e., to $\dot{Q}_{l,d,in}^i$ and $\dot{Q}_{l,d,out}^i$. On the other hand, the source term s refers to heat transfer on the r axis, i.e., to $\dot{Q}_{l_1 l_2,d}^i$, $\dot{Q}_{r,in}^i$, $\dot{Q}_{r,out}^i$ and \dot{Q}_e . The source term s also includes possible heat generation on conductors, expressed as $\dot{Q}_{g,1}$. The temperature distribution over space and time is represented in (18)–(21). Although (18)–(21) refer to only one of the GIL units, the same formulation applies for the remaining two units. GIL units are considered thermally isolated with each other.

$$\underbrace{\left(c_{v_{Air}} \rho_{Air} A_{r,1} \Delta z \right)}_{\text{coupling } c} \frac{\partial T_1^i}{\partial t} = \underbrace{\left(\dot{Q}_{1,d,in}^i - \dot{Q}_{1,d,out}^i \right)}_{\text{flux } f} + \underbrace{\dot{Q}_{12,d}^i}_{\text{source } s} \quad (18)$$

$$\left(c_{v_{Al}} \rho_{Al} A_{r,2} \Delta z \right) \frac{\partial T_2^i}{\partial t} = \dot{Q}_{2,d,in}^i - \dot{Q}_{2,d,out}^i - \dot{Q}_{12,d}^i + \dot{Q}_{23,d}^i + \dot{Q}_{r,in}^i + \dot{Q}_{g,2}^i \quad (19)$$

$$\left(c_{v_{SF_6}} \rho_{SF_6} A_{r,3} \Delta z \right) \frac{\partial T_3^i}{\partial t} = \dot{Q}_{3,d,in}^i - \dot{Q}_{3,d,out}^i - \dot{Q}_{23,d}^i + \dot{Q}_{34,d}^i \quad (20)$$

$$\left(c_{v_{Al}} \rho_{Al} A_{r,4} \Delta z \right) \frac{\partial T_4^i}{\partial t} = \dot{Q}_{4,d,in}^i - \dot{Q}_{4,d,out}^i - \dot{Q}_{34,d}^i + \dot{Q}_e - \dot{Q}_{r,out}^i + \dot{Q}_{g,4}^i \quad (21)$$

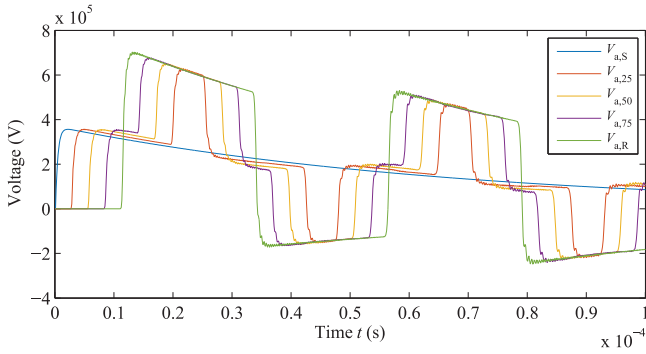


Fig. 5. Voltage response on first GIL conductor for LI.

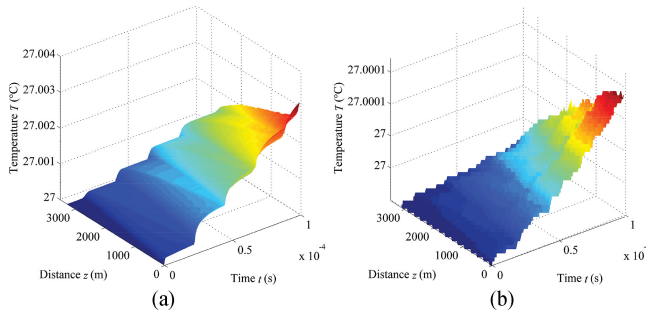


Fig. 6. Temperature distribution for LI setup. (a) Conductor. (b) Enclosure.

Note that coupling term c corresponds to the coupling of the partial derivatives with respect to time.

VI. SIMULATION RESULTS

A series of test cases are carried out to study the electro-thermal performance of the GIL. More specifically, the examined test cases include lightning surges, GIL energization as well as single-phase and three-phase short-circuits. All results illustrate the interaction of the thermal and electric fields, under varying transient simulation setups.

The GIL pul parameters are calculated at the dominant frequency of interest (f_{dom}), determined by the propagation velocity, the line length and the considered load [24]. Therefore, for the energization and lightning surge scenarios $f_{dom} = 22.106$ kHz, while for the short-circuit scenarios $f_{dom} = 44.212$ kHz.

A. Lightning Performance of the GIL

Lightning surges are simulated by connecting a double-exponential voltage source producing a 370 kV 1.2/50 μ s lightning impulse (LI) voltage [31] at the line sending end, whereas no load is connected to the line receiving ends. The applied voltage at the sending end of phase a of the GIL ($V_{a,S}$), as well as the voltage response for the same conductor at different points of the GIL is illustrated in Fig. 5. More specifically, $V_{a,25}$, $V_{a,50}$, $V_{a,75}$ and $V_{a,R}$ correspond to the voltage response at the 25%, 50%, 75% of the GIL length as well as at the receiving end of the first GIL conductor.

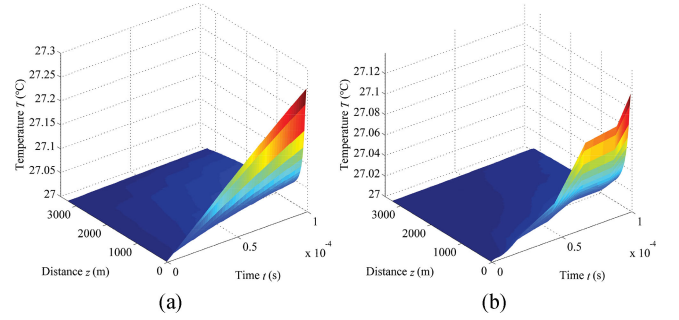


Fig. 7. Temperature distribution for GIL energization. (a) Conductor. (b) Enclosure.

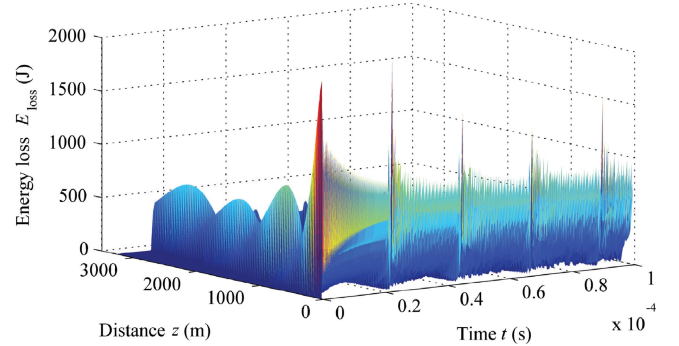


Fig. 8. Energy loss distribution in case of GIL energization.

Finally, in Fig. 6, the temperature distribution over space and time for the conductor and enclosure is indicated. Since the lightning surge is abrupt and therefore the total duration time of the event was 0.1 ms, only a marginal temperature increase on both metallic parts is observed. The temperature increase on the inner pipe and on SF_6 layers was even less significant, thus results are not illustrated.

Switching impulse (SI) scenarios have been also examined, verifying that in general impulse-related phenomena may not result into significant temperature increase at GIL layers.

B. GIL Energization

An ac voltage source of 275 kV is applied to the three GIL conductors at the sending end. Off-load conditions are examined. The temperature of all aluminum conductors prior to the GIL energization is 27 °C. As shown in Fig. 7, a marginal temperature increase of less than 1 °C is observed at the conductors and the corresponding enclosures. Although this increase is not expected to put the equipment at risk, thermal initialization at lower temperatures might be necessary for other setups i.e., for energization at higher voltage levels.

In Fig. 8, the energy loss E_{loss} distribution over space and time, in case of GIL energization, is illustrated. The transient at the first GIL segment, which is the one subject to energization, is more intense. That leads to a more significant E_{loss} and consequently to an apparent temperature increase at the beginning of the GIL, as seen in Fig. 7.

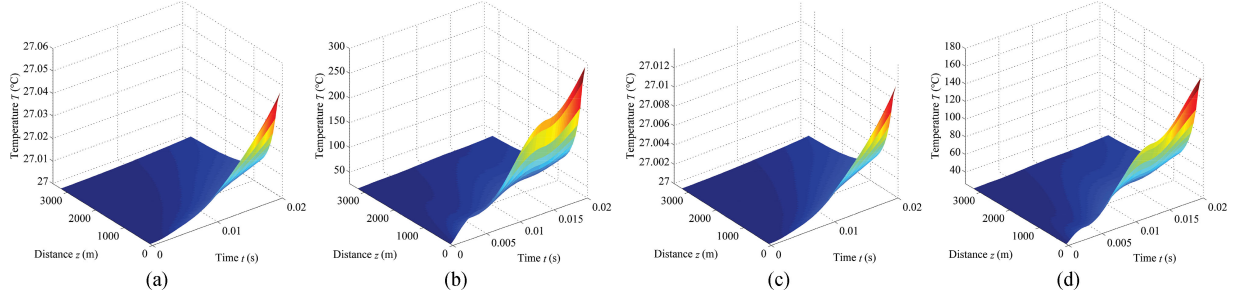


Fig. 9. Temperature distribution in case of single-phase short-circuit. (a) Inner pipe. (b) Conductor. (c) SF₆. (d) Enclosure.

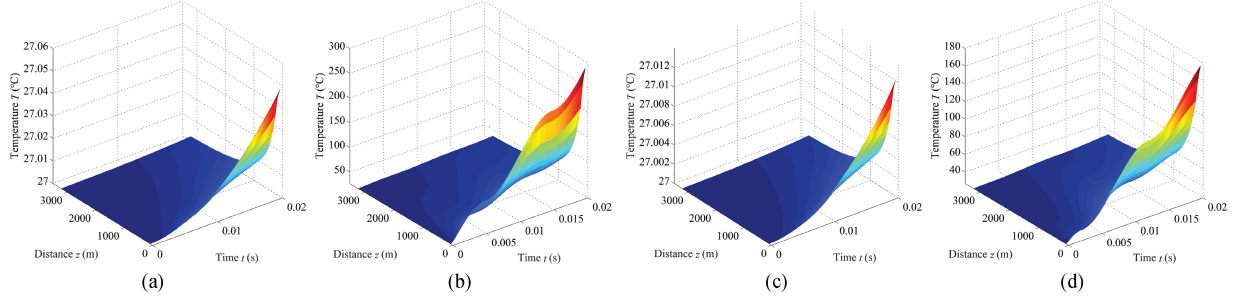


Fig. 10. Temperature distribution in case of three-phase short-circuit. (a) Inner pipe. (b) Conductor. (c) SF₆. (d) Enclosure.

C. Single-Phase Short-Circuit

A solid single-phase short-circuit is simulated assuming a 25 Ω load at the receiving end, corresponding to the pre-fault operating condition. The total simulation time is 20 ms, in order to capture the influence of slow transients on temperature distribution on all GIL layers. In Fig. 9, the temperature distribution over space and time for all layers is analyzed. During the simulation, a rapid temperature increase of more than 250 $^{\circ}\text{C}$ is observed on the conductor, whereas the outer enclosure is also affected by induced currents with an increase of almost 130 $^{\circ}\text{C}$. It is evident that in the case of short-circuits, the temperature of the inner pipe and SF₆ layers is also visibly affected. This test indicates a great impact on the temperature of all layers, especially on the metallic parts.

Moreover, based on the electro-thermal coupling process that is described in Section IV, useful conclusions about the variations of the conducting materials resistivity ρ can be drawn as well. In Fig. 10, resistivity variations for the GIL conductor over time and for variable cable segments in case of a single-phase short-circuit are illustrated. An interesting correlation between the results presented in Figs. 9(b) and 10 can be noted, revealing the interaction between the thermal and electrical parts. It is evident, that for the first GIL segments, where the resistivity increase is more sharp, the temperature increase is more evident. Additionally, the temperature over time increases with ρ .

D. Three-Phase Short-Circuit

A solid three-phase short-circuit scenario is also examined. The simulation setup is similar to the previous case. In Fig. 11(a), all GIL currents are illustrated. $I_{a,in}$, $I_{b,in}$ and $I_{c,in}$ correspond to

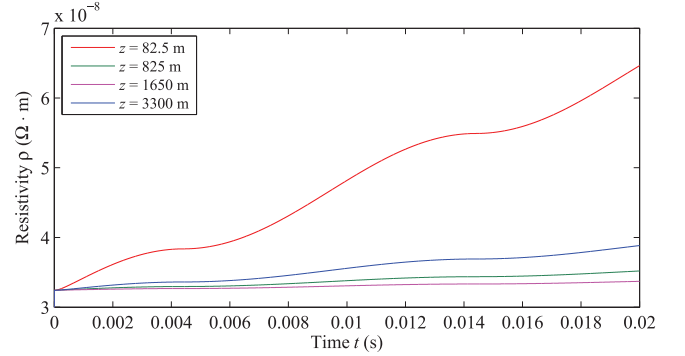


Fig. 11. Resistivity ρ in case of single-phase short-circuit.

the GIL conductor currents, whereas $I_{a,out}$, $I_{b,out}$ and $I_{c,out}$ refer to the induced currents on all three GIL enclosures. Fig. 11(b) indicates a zoom-in to the first part of the simulation to point out the transient response in the current, due to the short-circuit. Additionally, in Fig. 12 the temperature distribution over space and time is presented. As expected, since the currents in this test case are more intense, the conductor temperature is significantly increased, reaching almost 300 $^{\circ}\text{C}$, i.e., an increase of more than 950%. The outer enclosure temperature is also increased due to induced currents from 27 $^{\circ}\text{C}$ to about 175 $^{\circ}\text{C}$. Increase on inner pipe and SF₆ layers is less significant.

VII. DISCRETIZATION AND SOLVER EFFICIENCY

Multi-physics coupling problems are usually challenging in terms of computational burden, since time and space discretization should be properly determined in order both phenomena

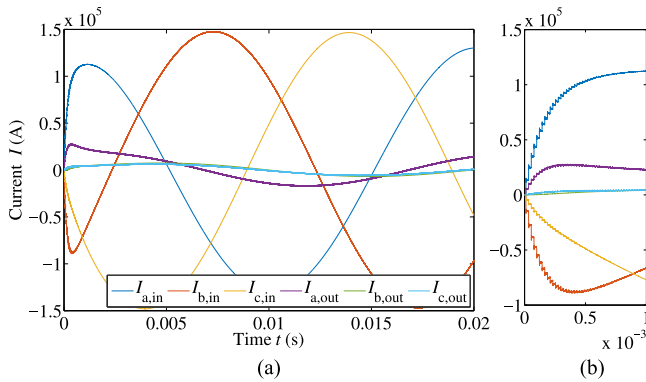


Fig. 12. GIL currents in case of three-phase short-circuit. (a) Full period. (b) Zoom.

to be captured. Therefore, simulation tools have to be not only accurate but time-efficient as well.

Considering the space discretization for the cases of lightning surges and GIL energization, 100 segments are used, i.e., for a total length of 3.3 km Δz equals 33 m, thus Δt is set to 0.11 μs . In the short-circuit scenarios, Δz and Δt are taken equal to 82.5 m and 0.275 μs , respectively.

Related to the discretization over time, as expected, the CFL condition presented in (15) has a significant impact on the overall computational burden. In other words, in order to simulate the examined electromagnetic transient phenomena over a period of 1 ms, Δt should be equal to $3.33 \cdot 10^{-8}$ s, which leads to long-lasting simulations. Proportionately, a smaller Δz will result to simulate more accurately possible local phenomena, e.g., a hot spot, a local deterioration of insulation or an arc in SF₆, but comes at the expense of increased computational effort. In this context, the option of non-uniform discretization is available with the proposed methodology, in order to select dense or sparse discretization for areas of high or low interest, respectively, or to take into consideration uneven distribution, the flow or the expansion of SF₆.

Note that, although the same discretization configuration considering only the electrical problem solution would require a simulation time of a few minutes, the solution of the thermal problem for every timestep and for all GIL layers leads to increased simulations. For the presented setup and considering MATLAB implementation, the computational burden varies from 4 to 90 hours, depending on the examined case, using an Intel Core i7-5500U, 2.4 GHz, RAM 8 GB PC.

Therefore, the ability of the proposed model to provide accurate results in a significantly reduced simulation duration, when compared with state-of-the-art software, constitutes a major advantage and contribution.

VIII. CONCLUSIONS

In this work, focus is given on coupled electro-thermal modeling of GILs, whereas a bi-directional mathematical formulation is proposed to that end. FDTD and VEM methodologies serve for simultaneous discretization over space and time and together with a time-efficient solver build a robust simulation tool for the transient analysis of GILs. The proposed approach

is non-specific and can be applied to any axisymmetric line configuration, given that expressions to describe heat transfer by any means are included.

The proposed approach can be used as a tool to identify safe operational ranges, without risk for equipment because of the temperature increase. A selection of intense electromagnetic transient scenarios are imposed in order to point out what will be the consequences in terms of temperature under worst-case conditions. Since the proposed approach calculates the temperature increase over time, this method can be also used to enhance the design and applicability of protection schemes to prevent equipment damage and aging.

Different transient conditions have been triggered in order the thermal response of the examined GIL configuration to be analyzed. The main conclusions can be summarized as:

- The short duration of lightning surges lead to negligible temperature increase along GILs.
- GIL energization leads to more observable but not dangerous to the equipment temperature increase, since the melting point of Aluminum (660 °C) is not expected to be reached.
- Short-circuits result into sharp temperature increase in the GIL conductors, even in the range of the melting point of Aluminum.

Experimental validation and results verification based on other approaches, e.g., FEM, are considered as future work.

REFERENCES

- [1] H. Koch, *Gas Insulated Transmission Lines (GIL)*. Hoboken, NJ, USA: Wiley, 2012.
- [2] T. Nojima, M. Shimizu, T. Araki, and H. Hata, "Installation of a 275 kV-3.3 km gas-insulated transmission line for underground large capacity transmission in Japan," in *Proc. Int. Conf. Large High Voltage Elect. Syst.*, 1998, pp. 1–3.
- [3] S. Kobayashi, N. Takinami, and A. Miyazaki, "Application of the world's longest gas insulated transmission line (GIL)," in *Proc. IEEE Power Eng. Soc. Gen. Meeting*, Jul. 2003, vol. 4, Jul. 2003, p. 2475.
- [4] R. Benato, E. M. Carlini, C. D. Mario, L. Fellin, A. Paolucci, and R. Turri, "Gas insulated transmission lines in railway galleries," *IEEE Trans. Power Del.*, vol. 20, no. 2, pt. 1, pp. 704–709, Apr. 2005.
- [5] R. Benato, C. D. Mario, and H. Koch, "High-capability applications of long gas-insulated lines in structures," *IEEE Trans. Power Del.*, vol. 22, no. 1, pp. 619–626, Jan. 2007.
- [6] D. Minaguchi, M. Ginno, K. Itaka, H. Furukawa, K. Ninomiya, and T. Hayashi, "Heat transfer characteristics of gas-insulated transmission lines," *IEEE Trans. Power Del.*, vol. PWRD-1, no. 1, pp. 1–9, Jan. 1986.
- [7] R. Benato, F. Dughiero, M. Forzan, and A. Paolucci, "Proximity effect and magnetic field calculation in GIL and in isolated phase bus ducts," *IEEE Trans. Magn.*, vol. 38, no. 2, pp. 781–784, Mar. 2002.
- [8] O. Volcker and H. Koch, "Insulation co-ordination for gas-insulated transmission lines (GIL)," *IEEE Trans. Power Del.*, vol. 16, no. 1, pp. 122–130, Jan. 2001.
- [9] A. Miyazaki *et al.*, "Line constant measurements and loading current test in long-distance 275 kV GIL," *IEEE Trans. Power Del.*, vol. 16, no. 2, pp. 165–170, Apr. 2001.
- [10] R. Benato and F. Dughiero, "Solution of coupled electromagnetic and thermal problems in gas-insulated transmission lines," *IEEE Trans. Magn.*, vol. 39, no. 3, pp. 1741–1744, May 2003.
- [11] D. A. Tsiamitros, T. A. Papadopoulos, and G. K. Papagiannis, "Modeling of gas-insulated lines buried in single and in two-layer earth," in *Proc. 44th Int. Univ. Power Eng. Conf.*, Sep. 2009, pp. 1–5.
- [12] R. Benato, P. Brunello, and L. Fellin, "Thermal behavior of EHV gas-insulated lines in Brenner pass pilot tunnel," *IEEE Trans. Power Del.*, vol. 25, no. 4, pp. 2717–2725, Oct. 2010.

- [13] S. W. Kim *et al.*, "Coupled finite-element-analytic technique for prediction of temperature rise in power apparatus," *IEEE Trans. Magn.*, vol. 38, no. 2, pp. 921–924, Mar. 2002.
- [14] D. Labridis and P. Dokopoulos, "Finite element computation of field, losses and forces in a three-phase gas cable with nonsymmetrical conductor arrangement," *IEEE Trans. Power Del.*, vol. 3, no. 4, pp. 1326–1333, Oct. 1988.
- [15] D. Labridis and V. Hatzianthassiou, "Finite element computation of field, forces and inductances in underground SF₆ insulated cables using a coupled magneto-thermal formulation," *IEEE Trans. Magn.*, vol. 30, no. 4, pp. 1407–1415, Jul. 1994.
- [16] D. I. Doukas, T. A. Papadopoulos, A. I. Chrysochos, D. P. Labridis, and G. K. Papagiannis, "Coupled electro-thermal transients simulation of gas-insulated transmission lines using FDTD and VEM modeling," in *Proc. Int. Conf. Power Syst. Transients*, Jun. 2017, pp. 1–6.
- [17] J. A. Souza, J. C. Ordóñez, R. Hovsapian, and J. V. C. Vargas, "Thermal modeling of helium cooled high-temperature superconducting DC transmission cable," *IEEE Trans. Appl. Supercond.*, vol. 21, no. 3, pp. 947–952, Jun. 2011.
- [18] C. R. Paul, *Analysis of Multiconductor Transmission Lines*. Hoboken, NJ, USA: Wiley, 2008.
- [19] C. G. Kaloudas, A. I. Chrysochos, and G. K. Papagiannis, "FDTD analysis of multiphase power cable systems using distributed constant parameters," in *Proc. MedPower 2014*, Nov. 2014, pp. 1–8.
- [20] R. D. Skeel and M. Berzins, "A method for the spatial discretization of parabolic equations in one space variable," *SIAM J. Sci. Stat. Comput.*, vol. 11, no. 1, pp. 1–32, 1990.
- [21] MATLAB, version 8.2.0.701 (R2013b). Natick, MA, USA: The Math-Works Inc., 2013.
- [22] D. I. Doukas, A. I. Chrysochos, T. A. Papadopoulos, D. P. Labridis, L. Harnefors, and G. Velotto, "Volume element method for thermal analysis of superconducting DC transmission cable," *IEEE Trans. Appl. Supercond.*, vol. 27, no. 4, pp. 1–8, Jun. 2017, Art. no. 5400608.
- [23] F. Rachidi, C. A. Nucci, and M. Ianoz, "Transient analysis of multiconductor lines above a lossy ground," *IEEE Trans. Power Del.*, vol. 14, no. 1, pp. 294–302, Jan. 1999.
- [24] A. I. Chrysochos, T. A. Papadopoulos, and G. K. Papagiannis, "Rigorous calculation method for resonance frequencies in transmission line responses," *IET Gen., Transm. Distrib.*, vol. 9, no. 8, pp. 767–778, 2015.
- [25] T. K. F. M. Tesche and M. V. Ianoz, *EMC Analysis Methods and Computational Models*. Hoboken, NJ, USA: Wiley, 1997.
- [26] R. Courant, K. Friedrichs, and H. Lewy, "Über die partiellen differenzengleichungen der mathematischen physik," *Mathematische Annalen*, vol. 100, no. 1, pp. 32–74, 1928.
- [27] P. Duthil, "Material properties at low temperature," in *Proc. CERN Accelerator School: Course Supercond. Accelerators*, 2015, p. 592.
- [28] *IEEE Standard of Common Requirements for High Voltage Power Switchgear Rated Above 1000 V*, IEEE Standard C37.100.1-2007, 2007.
- [29] *IEEE Standard for High Voltage Gas-Insulated Substations Rated Above 52 kV*, IEEE Standard C37.122-2010, 2011.
- [30] D. I. Doukas, A. I. Chrysochos, T. A. Papadopoulos, D. P. Labridis, L. Harnefors, and G. Velotto, "Coupled electro-thermal transient analysis of superconducting DC transmission systems using FDTD and VEM modeling," *IEEE Trans. Appl. Supercond.*, vol. 27, no. 8, pp. 1–8, Dec. 2017, Art. no. 5401608.
- [31] *Insulation Co-Ordination—Part 1: Definitions, Principles and Rules*, IEC Standard 60071-1:2006, 2006.



Theofilos A. Papadopoulos (S'01–M'09–SM'18) received the Dipl. Eng. and Ph.D. degrees from the School of Electrical and Computer Engineering, Aristotle University of Thessaloniki, Thessaloniki, Greece, in 2003 and 2008, respectively.

He is currently Assistant Professor with the Power Systems Laboratory, Department of Electrical and Computer Engineering, Democritus University of Thrace, Xanthi, Greece. His special interests are power systems modeling, PLC, and computation of electromagnetic transients.

Prof. Papadopoulos was the recipient of the Basil Papadias Award at the IEEE PowerTech '07 Conference.



Andreas I. Chrysochos (S'08–M'16) received the Dipl. Eng. and Ph.D. degrees from the School of Electrical and Computer Engineering, Aristotle University of Thessaloniki, Thessaloniki, Greece, in 2009 and 2015, respectively.

From 2015 to 2017, he was a Research Fellow with the same school. Since 2017, he has been a Senior Engineer with the R&D Department, Cable Hellenic Cables S.A., Viohalco Group, Korinthos, Greece. His special interests include power systems modeling, computation of electromagnetic transients,

and PLC.

Dr. Chrysochos was a scholar of the Alexander S. Onassis Public Benefit Foundation (2012–2015, 2016–2017).



Dimitris P. Labridis (S'88–M'90–SM'00) received the Dipl.-Eng. and Ph.D. degrees from the Department of Electrical Engineering, Aristotle University of Thessaloniki, Thessaloniki, Greece, in 1981 and 1989, respectively.

Since 1986, he has been with the Electrical Engineering Department, Aristotle University of Thessaloniki, where he is currently a Professor. His research interests include power system analysis with a special emphasis on the simulation of transmission and distribution systems, smart grids, distributed energy

resources, power line communications, coupled electromagnetic and thermal field analysis, interference of power transmission and distribution lines, artificial intelligence applications in power systems, and applied superconductivity.



Dimitrios I. Doukas (S'13–M'17) received the Dipl. Eng. and Ph.D. degrees in electrical and computer engineering from the Aristotle University of Thessaloniki, Thessaloniki, Greece, in 2009 and 2017, respectively, and the M.Sc. degree in sustainable energy systems from the University of Edinburgh, Edinburgh, U.K., in 2011.

From 2011 to 2013, he was with ABB Corporate Research, Västerås, Sweden, and since 2017 he has been with NET2GRID B.V., Zeist, The Netherlands.

His research interests include applied superconductivity, energy storage, and power system analysis and control.



Grigoris K. Papagiannis (S'79–M'88–SM'09) received the Dipl. Eng. and the Ph.D. degrees from the School of Electrical and Computer Engineering, Aristotle University of Thessaloniki, Thessaloniki, Greece, in 1979 and 1998, respectively.

He is currently a Professor with the Power Systems Laboratory, School of Electrical and Computer Engineering, Aristotle University of Thessaloniki. His special interests include power systems modeling, computation of electromagnetic transients, distributed generation, and PLC.